Earth and Planetary Science Letters, 72 (1985) 311–326
Elsevier Science Publishers B.V., Amsterdam – Printed in The Netherlands

[1]

Evidence for oxidizing conditions in the solar nebula from Mo and W depletions in refractory inclusions in carbonaceous chondrites

Bruce Fegley, Jr. [1,2] and Herbert Palme [2]

[1] *Department of Earth, Atmospheric and Planetary Sciences and Ceramics Processing Research Laboratory, Massachusetts Institute of Technology, Cambridge, MA 02139 (U.S.A.)*

[2] *Max-Planck-Institut für Chemie (Otto-Hahn-Institut), Saarstrasse 23, 6500 Mainz (F.R.G.)*

Received September 19, 1984
Revised version received December 3, 1984

Depletions of Mo and W relative to other refractory metals of similar volatility (Re, Os, Ir, Ru, Pt) are common in a suite of 16 Ca,Al-rich inclusions (CAIs) from 5 carbonaceous chondrites. Twelve of the 16 CAIs from Allende, Grosnaja, Leoville, and Ornans show Mo depletions; six of these 12 inclusions also show W depletions. The one CAI analyzed from the Essebi chondrite shows no depletions. The Mo and W depletions have a very characteristic pattern with Mo always more depleted than W. The same Mo and W depletion pattern occurs in calculated refractory metal alloy compositions formed at oxygen fugacities 10^3 to 10^4 times greater than the canonical solar nebula oxygen fugacity. We conclude that Mo and W depletions are common in CAIs from carbonaceous chondrites and that the depletions result from high temperature oxidation. The oxidation may have occurred during the evaporation of primitive dust into CAIs but is also consistent with condensation at high oxygen fugacities. No potential alternative processes appear to be capable of producing the observed Mo and W depletion patterns.

1. Introduction

Many Ca,Al-rich inclusions (CAIs) in Allende and other carbonaceous chondrites have high concentrations of refractory metals (W, Re, Os, Ir, Mo, Ru, Pt). These elements are enriched to 15–30 × chondritic abundances ([1,2] and references therein). Enrichment factors of the rare earth elements (REE) and other refractory lithophile trace elements (e.g., Sc, Ba, Zr, Nb, Th, U, etc.) are similar. In many inclusions refractory metals are not uniformly enriched, but their abundances appear related to their volatility [3,4]. Thus, in an "ultra"-refractory inclusion, which represents either a high-temperature evaporation residue or an initial condensate, very refractory metals (Re and Os) are more enriched than less refractory metals (Ru and Pt) [5]. Similar, although not as extreme, abundance patterns consistent with the vapor pressures of the refractory metals (W < Re ≈ Os < Ir ≈ Mo < Ru < Pt) have been reported in metal grains from Allende CAIs by Blander et al. [3] and Wark [6].

However, Mo and W do not always fit into this pattern. They are commonly more depleted than expected from their relative volatilities. Because W has the lowest vapor pressure of these metals and Mo has a vapor pressure very similar to that of Ir, these depletions are not a vapor pressure effect. Palme et al. [5,7] and Wark and Wasserburg [8] have suggested that anomalously low concentrations of Mo and W in CAIs indicate the loss of these elements as volatile oxides.

In this paper, we present evidence that Mo and W depletions are common in CAIs in carbonaceous chondrites. We also attempt to show that the depletions are consistent with high temperature equilibration of the refractory metals in a relatively oxidizing environment, i.e., at oxygen fugacities several orders of magnitude greater than the canonical solar nebula oxygen fugacity. Finally, we discuss several scenarios for producing the

0012-821X/85/$03.30

observed Mo and W depletions, and some implications for the formation of CAIs in carbonaceous chondrites.

2. Refractory metal abundances in refractory inclusions

Abundances of W, Re, Os, Ir, Mo, Ru, and Pt in refractory inclusions from the Allende (CV3), Essebi (CM2), Grosnaja (CV3), Leoville (CV3), and Ornans (CO3) chondrites have been determined by neutron activation analysis at Mainz [9]. The analytical data for 16 inclusions of various mineralogical types and REE groups have been examined in this work. Wark and coworkers have measured the concentrations of W, Re, Os, Ir, Mo, Ru, Pt, and Rh in refractory metal nuggets in several CAIs in Allende and Leoville. These analyses, which were done by energy-dispersive spectroscopy (EDS) with a scanning electron microscope (SEM), are summarized by Wark [6]. Blander and coworkers also reported refractory metal nugget compositions (determined by EDS/SEM and electron microprobe) in several Allende inclusions [3,10]. Several groups have determined (by neutron activation analysis and spark source mass spectrometry) the abundances of various subsets of the refractory metals W, Re, Os, Ir, Mo, Ru, and Pt in Allende and Murchison (CM2) inclusions (see references cited in [1,2]). However, because all 7 elements were not analyzed simultaneously in any of these CAIs, Mo and W depletions cannot be determined from the available data.

Our analysis of the Mainz neutron activation results shows that 12 out of 16 inclusions studied have Mo depletions (relative to the C1-normalized refractory metal ratios or enrichments). Six of the 12 inclusions also have W depletions, but there is no inclusion which is depleted in W without *also* being depleted in Mo. Mo depletions are char-

TABLE 1

Selected analytical data for refractory metals (Mo, W depletions italicized)

Sample	Classification [a]	C1 normalized abundance (Os = 1.0)							Os (ppm)
		W	Re	Os	Ir	Mo	Ru	Pt	
A4 [b]	Type B, Group I	1.2	1.4	1.0	1.6	1.2	0.83	1.3	6.5
3529-Z [c,d]	Type B, Group I	0.85	0.97	1.0	0.91	*0.75*	1.0	0.54	7.1
AM-1 [c]	Type A, Group VI	0.87	1.0	1.0	0.92	*0.71*	0.96	0.64	17.7
3898 [c]	"FUN", Group I	0.85	0.92	1.0	0.96	*0.61*	0.96	0.61	8.2
A17 [c]	Type B, Group I	1.1	0.89	1.0	1.0	*0.40*	1.3	0.94	6.1
Grosnaja [e]	Type B, Group I	*0.75*	1.0	1.0	1.0	*0.38*	1.2	0.69	5.6
TE [e,f]	"FUN", Group I	*0.18*	0.62	1.0	0.91	*< 0.06*	0.82	< 0.14	7.2
Leo-1 [g]	Type B, Group I	*0.56*	0.93	1.0	0.92	*0.23*	0.79	0.22	7.7
Leo-1FR [h]	Fremdling	*0.49*	1.1	1.0	0.95	*0.028*	0.36	0.078	2.16%
Ornans [i]	Fremdling	*0.038*	1.0	1.0	0.99	*< 0.088*	0.25	0.024	0.74%
A14Fr [k]	Fremdling	0.80	0.90	1.0	0.89	0.74	0.71	0.97	0.40%

Refractory inclusions are from Allende unless noted otherwise.

[a] Mineralogical and REE classification schemes are discussed in references 1, 2, and 4.

[b] Wänke et al. [12], revised data.

[c] Palme et al. [9].

[d] Mason and Taylor [4] analyzed 3529-Z by spark source mass spectrometry; their data for Re, Os, Ir, Ru, Pt are in good agreement with present data.

[e] El Goresy, Palme, and Bukovanska, in preparation.

[f] Dominik et al. [13] and Clayton et al. [14] give petrologic and isotopic data for TE. This inclusion is forsterite rich.

[g] Palme and Wlotzka [15].

[h] Metal and phosphate Fremdling in inclusion Leo-1. Data are plotted in Palme et al. [5].

[i] "Ultra"-refractory inclusion in Ornans [5].

[k] Palme and Wlotzka [11]. Fremdling bulk composition from neutron activation analysis.

acterized by Cl-normalized Mo concentrations lower than those for Ir and Ru; W depletions are similar (low W abundances relative to the Re and Os abundances). The observed depletions are outside conservative estimates of analytical uncertainties, which are < 5% for Ir, Re, Os; 5–10% for W, Mo, Ru; and 10–30% for Pt [5,9,11].

Selected refractory metal analyses of CAIs in Allende and other chondrites are listed in Table 1. Data are presented as abundances relative to Cl values [16], normalized so that the Os enrichment in each inclusion is set equal to 1.0. Enrichments relative to Cl can be recalculated from the normalized abundances and the Os concentration in each inclusion, which is also given in the table. An Allende CAI (A4) with an essentially unfractionated metal abundance pattern (i.e., approximately equal enrichments of all refractory metals) is also shown for comparison.

These data plus literature data [3,6,10,17] illustrate several important points. First, there is a wide range of Mo depletions. Some inclusions have Mo depletions of the order of 25% while others have depletions of $\geqslant 30\times$.

Second, W depletions also occur in several inclusions. They are always associated with Mo depletions (the converse is not true). The size of the W depletion is also correlated with the size of the Mo depletion: CAIs with large Mo depletions also have large W depletions.

Third, Mo and W depletions are widespread. They occur in CAIs in four carbonaceous chondrites: Allende, Grosnaja, Leoville, and Ornans. Seven out of 10 from Allende show Mo depletions: four of these are Type B CAIs with essentially unfractionated (Group I) REE patterns; AM-1 is a "fluffy" Type A [1]; TE is a forsterite-rich FUN inclusion [13,14]; and 3898 is a possible FUN inclusion [18]. All three Leoville CAIs analyzed show Mo and W depletions. Only one inclusion from Grosnaja (Type B) and one from Ornans (an "ultra"-refractory Fremdling) have been analyzed and both show Mo and W depletions. The only CAI from Essebi which has been analyzed has an essentially unfractionated refractory metal abundance pattern: Mo and W are not depleted [17]. Our analysis of Wark's [6] mean composition for the refractory metal nuggets in the core of the Type A Allende inclusion 3643 also shows Mo and W depletions. Thus, Mo and W depletions apparently are common in Type B Allende inclusions (4 of 7 analyzed), and also occur in every type (i.e., A, B, FUN, "ultra"-refractory) analyzed. However, only single CAIs of some types have been analyzed and not all mineralogical and REE types have been studied. Therefore, the possibility that some types of CAIs consistently are *not* depleted in Mo and W cannot be tested.

Fourth, Mo and W depletions apparently are independent of the REE abundance pattern: Mo and W depletions occur in CAIs with group I, II, and VI REE patterns. However, only one group II and one group VI were analyzed and no data are available for any group III and V CAIs.

Fifth, Mo and W depletions occur in several FUN inclusions. EDS/SEM analyses of refractory metal nuggets show Mo and W depletions in C1 (Type B, Group I) and a Mo depletion (no W analyses done) in Egg 3 (a mixture of Types B and A, Group I) [6]. Other FUN inclusions, e.g., EK141, HAL, and CG14, cannot be evaluated because the necessary analytical data are not available.

Last, there is no apparent correlation between Mo and W depletions in refractory inclusions and the alteration processes which have introduced Fe, Na, and Cl into refractory inclusions. We compared Fe, Na, and Cl concentrations in 16 inclusions with and without Mo and W depletions, using data from several sources [4,9,12,15,17,19]. These data show that Fe, Na, and Cl concentrations in inclusions showing depletions are in the same range as Fe, Na, and Cl concentrations in CAIs that do not show Mo and W depletions.

3. Calculation of the composition of refractory metal alloys

We calculated the composition of refractory metal alloys for a large range of temperatures, pressures, and oxygen fugacities to test the hypothesis that Mo and W depletions in refractory inclusions are due to loss of these two elements as volatile oxides [5,7,8]. These calculations extend previous calculations of alloy compositions [3,5,11]

and agree very well with them where the calculations overlap.

3.1. Method of calculation

Refractory metal alloy compositions were calculated using a multicomponent gas-solid chemical equilibrium code (METKON) originally developed by H. Palme, J.W. Larimer, and H. Kruse [11]. METKON operates subject to the dual constraints of mass balance and chemical equilibrium. A set of equations is considered:

$$P_M(\text{alloy}) = P_M(\text{nebula}) \quad (1)$$

where P_M(alloy) and P_M(nebula) are the partial pressures over the alloy and in the nebula, respectively. P_M(alloy) is related to the thermodynamic activity of M in the alloy ($a_M = \gamma_M X_M$) and to the vapor pressure (P_M°) of pure M(s,liq) by the equation:

$$P_M(\text{alloy}) = a_M P_M^\circ \quad (2)$$

The amount of each element in the alloy can be expressed as a fraction of the solar abundance (relative to Si = 10^6) of each element. Thus, equation (2) can be rewritten:

$$P_M(\text{alloy}) = \gamma_M P_M^\circ \left[F_M A(\text{M}) / \sum F_i A(i) \right] \quad (3)$$

where the F_i's are the fractions of metal atoms which are condensed, $A(i)$ is the solar abundance of element i; the F_i's are the unknowns. One such equation is required for every metal M in the alloy and the present calculations are for a 13-component alloy. The set of non-linear equations is solved by a Newton-Ralphson iteration technique for the 13 unknown F_i's [20].

In order to solve the equation set it is also necessary to calculate the partial pressures of each of the metals in the gas. Some elements, such as W and Mo, may exist as metals *and* metal oxides in the solar nebula [3,5,11]. Others (such as Re, Os, Fe, and Cr) exist as gaseous metals but may form metal oxides at higher oxygen fugacities. P_M(nebula) can be calculated from:

$$P_M(\text{nebula}) = \left[A(\text{M}) / A(\text{H}_2 + \text{He}) \right] \times (1 - F_M) P_{\text{total}} f_M \quad (4)$$

where $A(H_2 + He)$ is the sum of the solar abundances of H_2 and He, P_{total} is the total pressure, and f_M is defined by the equation:

$$f_M = P_M / P_{\Sigma M} \quad (5)$$

$P_{\Sigma M}$ is equal to the sum of the partial pressures of all gases containing element M. To maintain mass balance each partial pressure term in this sum must be multiplied by the number of M atoms in that species. For example, the partial pressure sum for W is written as:

$$P_{\Sigma W} = P_W + P_{WO} + P_{WO_2} + P_{WO_3} + 2P_{W_2O_6} + 3P_{W_3O_8} + 3P_{W_3O_9} + 4P_{W_4O_{12}} \quad (6)$$

Each partial pressure term can in turn be expressed in terms of the equilibrium constant for forming that gas from its constituent elements. The partial pressure of MoO(gas) for example can be written as:

$$P_{MoO} = a_{Mo} P_{O_2}^{1/2} K(\text{MoO}) \quad (7)$$

where K(MoO) is the equilibrium constant for forming MoO(gas) from the constituent elements in their respective reference states. Similar equations are written for each gas in the partial pressure sum of each element. The a_i terms are the unknowns for which the partial pressure sums are then solved at a predetermined oxygen fugacity. Again, this is done by a successive iteration technique. Once the elemental activities are known, the partial pressures of the various metallic gases and the refractory metal alloy composition can be calculated. It is important to note that the gas phase and gas-solid equilibrium calculations are coupled because the fraction of element i which is condensed (F_i) appears in both equations (3) and (4). Therefore, the two sets of calculations must be done simultaneously using iterative techniques [20].

The 13 elements included in the present calculations were Fe, Ni, Pt, Ru, Ir, Mo, Re, Os, W, Rh, Co, Pd, and Cr. Elemental abundances are taken from Anders and Ebihara [16] and vapor pressures of the elements from Hultgren et al. [21]. Vapor pressures of several elements are also given in the JANAF Tables [22]. These values are not significantly different from those in Hultgren and our conclusions are not affected by the data used. All 37 metallic and oxide gases for which data are

TABLE 2

Thermodynamic data for selected oxide gases [log $K = A/T + B$]

Gas	A	B	Sources
CoO	−16,164	5.71	[23]
IrO_3	−993.4	−2.30	[24]
Ir_2O_3	−15,865	5.93	[24]
NiO	−15,542	4.60	[23,25]
OsO_4	17,240	−7.49	[23,25]
PdO	−18,227	4.03	[26]
PtO_2	−8,585	0.20	[27]
Re_2O_7	57,478	−18.6	[26]
RhO_2	−9,866	1.08	[27]
RuO_4	9,647	−7.88	[23,28]

available were included in these calculations. Data for the following oxide gases are from the JANAF Tables and subsequent supplements [22]: CrO, CrO_2, CrO_3, FeO, MoO, MoO_2, MoO_3, WO, WO_2, WO_3, W_2O_6, W_3O_8, W_3O_9, W_4O_{12}. Data for oxide gases of Co, Ir, Ni, Os, Pd, Pt, Re, Rh, and Ru are from a variety of sources. The oxide gases, thermodynamic data used, and literature sources are listed in Table 2. All data from Hultgren and the JANAF Tables have been fit to linear equations of the form $\log K = A/T + B$ where K is the equilibrium constant for formation from the elements in their respective reference states. (The vapor pressure of a pure element is equal to the equilibrium constant K.)

3.2. *Refractory alloy compositions at canonical solar nebula oxygen fugacities*

The calculations, which assume ideal solid solution ($\gamma = 1.0$) in the multicomponent alloy, were done at total pressures from 10^{-3} to 10^{-12} bars and at temperatures from 2000 to 800 K. The oxygen fugacity, calculated from the H_2O and H_2 fugacities in the solar nebula, varied from $\approx 10^{-14.4}$ at 1900 K to $\approx 10^{-19.3}$ at 1400 K.

Our results agree with previous calculations at 10^{-3} and 10^{-4} bars pressure [3,11]. In particular, we confirm the conclusion of Palme et al. [5] that there is a close match (see [5, fig. 6]) between observed and calculated compositions for alloys with smooth, volatility controlled abundance patterns, e.g., the nuggets analyzed by Blander et al. [3]. This match indicates that the ideal solution assumption is a good first approximation, at least for Ir, Mo, and Ru.

The fragmentary data available on activity coefficients also serve as an indicator of possible effects of non-ideality in the refractory metal alloys. Fraser and Rammensee [29] found $\gamma_{Co} \approx 1$ in Fe-Ni-Co alloys. Mass spectrometric activity measurements for Ni, Co, Cr, and V in synthetic refractory metal alloys gave γ's in the range ≈ 0.4–2.5 at 1600 K [30]. The alloys had compositions similar to the calculated composition of a 1500 K alloy [11]. Although slightly larger deviations from ideality may occur at lower temperatures, the activity coefficients will still be close to unity. More details are given by Rammensee et al. [30]. Gibson [31] found $\gamma_W \approx 0.3$ in a 9.5 at.% W-Ir alloy at 2237 K and $\gamma_W \approx 7.3$ in a 0.4 at.% W-Os alloy at 2216 K. Setting $\gamma_W = 7$ in some calculations resulted in negligible changes (≈ 2 wt.%) in the W concentration in high-temperature W-Re-Os alloys. These changes rapidly disappeared at temperatures below 1900 K. No activity coefficient data are available for Mo- and W-bearing multicomponent alloys. Fuchs and Blander [10] suggested that bcc Mo and W may segregate from hcp Os, Ru, and Re. However, the occurrence of CAIs and metal nuggets which are not depleted in Mo and W but which have volatility controlled abundance patterns suggests that this segregation is not important [3,6]. Furthermore, the Mo-Os, Mo-Ru, and Mo-Re phase diagrams [32] show extensive (10 40 at.%) Mo solubility in these metals. Further information about the possible effects of non-ideality is given in Palme and Wlotzka [11]. Although complete activity coefficient data are not available, the existing data indicate that non-ideality effects are small and do not significantly affect our results.

If Mo and W oxide solid solution in refractory oxide and silicate minerals (e.g., perovskite and melilite) were important, significant amounts of the Mo and W in CAIs would be found in these minerals and oxide solid solution terms would have to be included in equation (4). However, the observed refractory metal concentrations in CAIs can be accounted for by the observed metal nug-

gets [6]. Also, extensive analyses of mineral separates from Allende and Leoville CAIs do not show W or Mo in these minerals (H. Palme, unpublished results). Although no perovskites were analyzed, analysis of a light-REE-enriched terrestrial perovskite (Kaiserstuhl area) showed no W (B. Spettel, private communication). In fact, Mo and W oxide activity coefficients in perovskite and melilite may be very large.

Ideal solid solution calculations considering all solid Mo and W oxides show that only negligible amounts of Mo dissolve in perovskite at 1650 K and 10^{-3} bars (0.02% at $H_2O/H_2 = 5 \times 10^{-4}$ and 0.12% at $H_2O/H_2 = 0.1$). Larger amounts of W dissolve in perovskite under the same conditions (17.5% and 10.9% respectively). Less W dissolves in perovskite as the oxygen fugacity increases because of the large volatility of W oxides. However, CAI analyses, crystal chemistry, and terrestrial geochemistry of Mo and W all indicate that ideal solution of Mo and W oxides in perovskite (or melilite) is a poor assumption; the actual activity coefficients are probably much larger. Thus, Mo and W oxide solid solution was neglected in our calculations.

Table 3 summarizes some of our results, expressed as 50% condensation temperatures for the metals in the multicomponent alloy. The 50% condensation temperatures at intermediate pressures are easily calculated from the data in Table 3 because $1/T$ vs. log P plots are linear. The initial condensation point of the alloy is (arbitrarily) defined as the temperature where 1 part in a thousand of total Re is condensed. Using this definition, the refractory alloy first forms at the following temperatures: 1926 K (10^{-3} bars), 1683 K (10^{-6} bars), and 1497 K (10^{-9} bars). Comparison of these temperatures and the data in Table 3 with the refractory mineral condensation temperatures in Kornacki and Fegley [33] shows that metal alloys are always stable to higher temperatures than refractory minerals over the pressure range considered at canonical solar nebula oxygen fugacities. This is an important constraint on formation models for refractory inclusions [2,33].

TABLE 3

50% condensation temperatures (ideal solid solution)

Metal	50% condensation temperature at different total pressures (K)		
	10^{-3} bars	10^{-6} bars	10^{-9} bars
W	1892	1625	1415
Re	1905	1666	1485
Os	1897	1663	1482
Ir	1683	1465	1295
Mo	1675	1456	1270
Ru	1642	1432	1268
Pt	1490	1275	1125
Rh	1475	1250	1100
Co	1448	1202	1026
Ni	1446	1201	1026
Fe	1428	1185	1013
Pd	1415	1165	988
Cr [a]	1390	1154	986

[a] No solid Cr-bearing oxides considered in these calculations.

3.3. *Refractory alloy compositions at higher oxygen fugacities*

Extensive calculations of refractory alloy compositions were done at oxygen fugacities higher (i.e., more oxidizing) than the canonical solar nebula oxygen fugacity. The higher oxygen fugacities can be expressed in several equivalent ways; in anticipation of the later discussion of mechanisms, we use the (H_2O/H_2) ratio as the parameter to represent f_{O_2}. For reference, the H_2O/H_2 ratio

TABLE 4

Oxidation sequence for refractory metals (50% of metal = M(gas), 50% = metal oxide gases, 1600 K and 10^{-3} bars)

Metal	$\log_{10}(H_2O/H_2)$	$\log_{10} f_{O_2}$
W	−6.6	−23.5
Mo	−2.9	−16.2
Re	−0.18	−10.7
Os	−0.05	−10.4
Cr	0.18	−10.0
Ir	1.5	−7.4
Fe	2.2	−6.0
Ru	2.3	−5.7
Pt	2.4	−5.6
Rh	2.6	−5.2
Co	3.1	−4.1
Ni	3.9	−2.4
Pd	6.7	+3.0

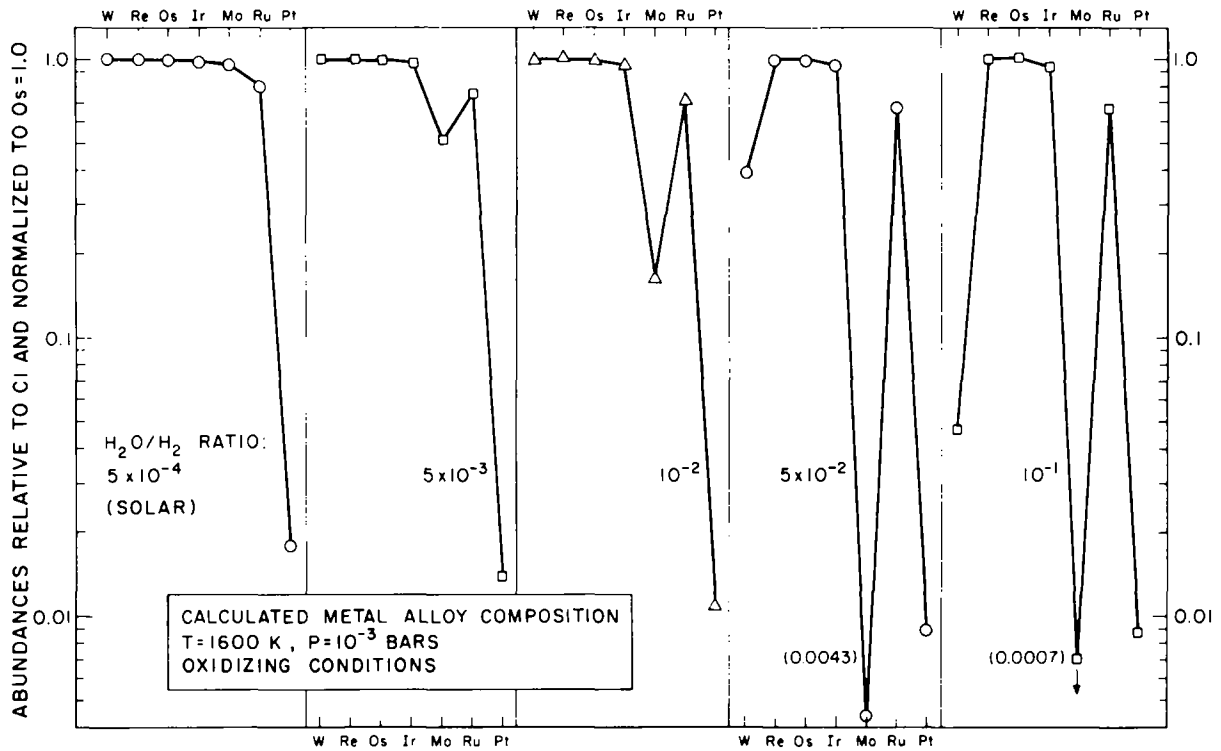

Fig. 1. Mo and W depletions in refractory metal alloys as a function of oxygen fugacity at constant temperature and pressure. The oxygen fugacity is expressed as the (H_2O/H_2) ratio, and can be calculated from $\log_{10}K(H_2O, g)$ in JANAF [22].

corresponding to the canonical solar nebula oxygen fugacity is $\approx 5 \times 10^{-4}$.

Table 4 and Fig. 1 illustrate the effects of variable oxygen fugacities on the chemistry of the refractory metals. Table 4 shows the oxygen fugacities at which 50% of each of the metals is monatomic gas and 50% of each is metal oxide gases. Only the gas phase chemistry is considered in order to show a relative oxidation sequence for all the metals. Fig. 1 illustrates the effect of increasing oxygen fugacity at constant temperature and pressure (1600 K, 10^{-3} bars) on the composition of the refractory metal alloy.

The alloy at the solar (H_2O/H_2) ratio is depleted in Ru and Pt relative to chondritic abundances. This is in accord with the relative volatilities listed in Table 3. However, as the (H_2O/H_2) ratio (and thus f_{O_2}) is increased, marked irregularities appear in this smooth pattern. An increase in the (H_2O/H_2) ratio by an order of magnitude produces a noticeable Mo depletion ($\approx 50\%$ relative to chondritic abundance). Further increases in the (H_2O/H_2) ratio yield progressively greater Mo depletions. At a (H_2O/H_2) ratio of 0.1 ($f_{O_2} = 10^{-12.3}$ vs. $10^{-16.9}$ for the solar nebula) the amount of Mo in the alloy relative to the chondritic abundance is $\approx 7 \times 10^{-4}$. Still larger Mo depletions occur at higher (H_2O/H_2) ratios.

Furthermore, Fig. 1 also illustrates that increased oxygen fugacities also lead to W depletions in refractory metal alloys. However, W depletions do not appear until oxygen fugacities at which substantial Mo depletions already exist. Further increases in oxygen fugacity then lead to larger W depletions. However, it is important to note that Mo depletions are *always* larger than the corresponding W depletions in the same alloy.

The highly specific nature of Mo and W depletions in metal alloys is easily understood as an interplay between two factors: the vapor pressure

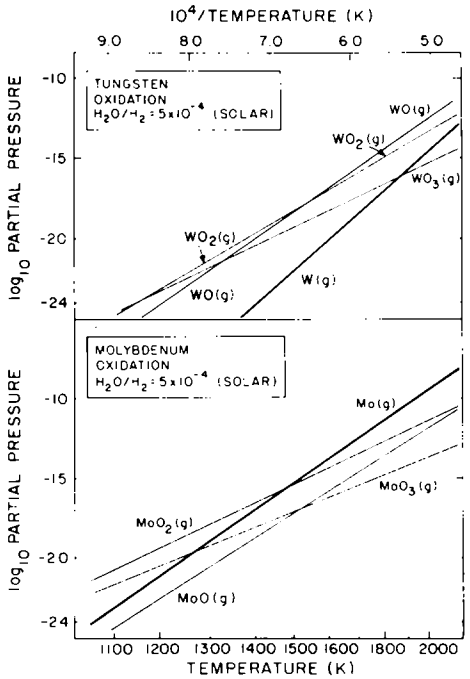

Fig. 2. Gas chemistry over solid W and solid Mo. W is more easily oxidized than Mo and is also more refractory. The results are for the canonical solar nebula oxygen fugacity.

of metal and the tendency of metal atoms in the gas phase to be oxidized. Although W is more easily oxidized than Mo (and thus might be expected to be depleted to a greater extent than Mo) it is also more refractory than Mo. The refractory nature of W is reflected in the lower vapor pressure of W compared to Mo [21].

The tendency of W to be more easily oxidized than Mo is illustrated in Fig. 2 which shows the gas phase equilibria for the two elements. A comparison of these equilibria at 1600 K and 10^{-3} bars shows that at the canonical solar nebula oxygen fugacity ($H_2O/H_2 = 5 \times 10^{-4}$) the ratio of W(g) to all W-oxide gases is only 3.6×10^{-4} while the corresponding ratio of Mo(g) to all Mo-oxide gases is approximately 6. At constant temperature and pressure the $M(g)/\Sigma MO(g)$ ratios for W and Mo exhibit the expected behavior with respect to changes in the oxygen fugacity: both decrease with increasing oxygen fugacity and increase with decreasing oxygen fugacity. However, under *all P, T,* f_{O_2} conditions the ratio of W(g) to all W-oxide gases is always smaller (generally by orders of magnitude) than the ratio of Mo(g) to all Mo-oxide gases.

The general shape of the calculated metal alloy abundance patterns in Fig. 1 is very similar to the shape of the metal abundance patterns observed in the refractory inclusions showing Mo and W depletions. This similarity suggests that the latter patterns might result from high-temperature oxidation of the metals in refractory inclusions.

3.4. Comparison of observed and calculated refractory metal abundance patterns

Some comparisons between calculated and observed metal abundance patterns are shown in Figs. 3-6. The calculations in Figs. 3–6 are all at a total pressure of 10^{-3} bars to facilitate comparison with other work on major and trace element condensation, which has generally been done at 10^{-3} bars (see references in [1,2]). Equivalent results are obtained in all cases at lower pressures, except that

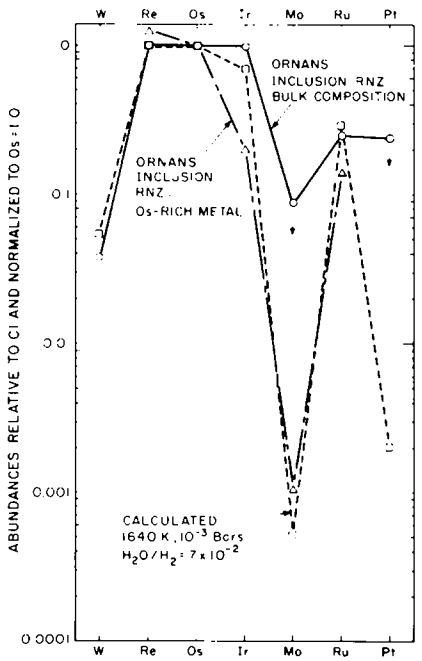

Fig. 3. Observed and calculated refractory metal abundances in Ornans inclusion RNZ [5]. The bulk composition (see Table 1) is from neutron activation; the Os-rich metal composition is from electron microprobe analysis.

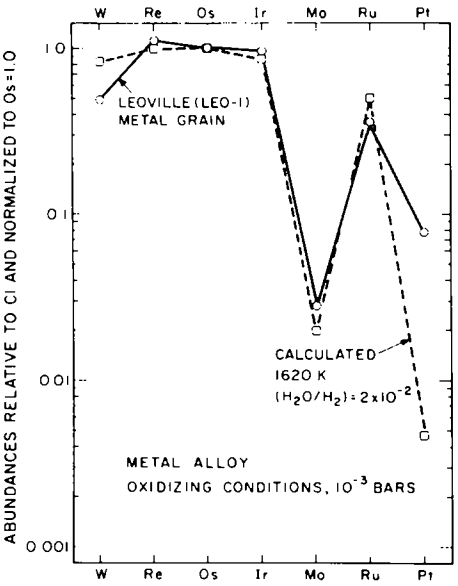

Fig. 4. Observed and calculated refractory metal abundances in a big metal grain from Leoville inclusion Leo-1 [5,15]. The composition (see Table 1) is from neutron activation. This grain, which also contains phosphate, may be a Fremdling.

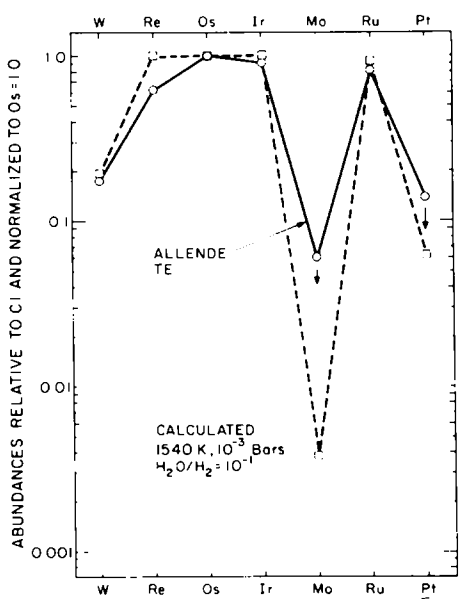

Fig. 5. Observed and calculated refractory metal abundances in the Allende FUN inclusion TE [13,14]. The bulk composition from neutron activation is in Table 1.

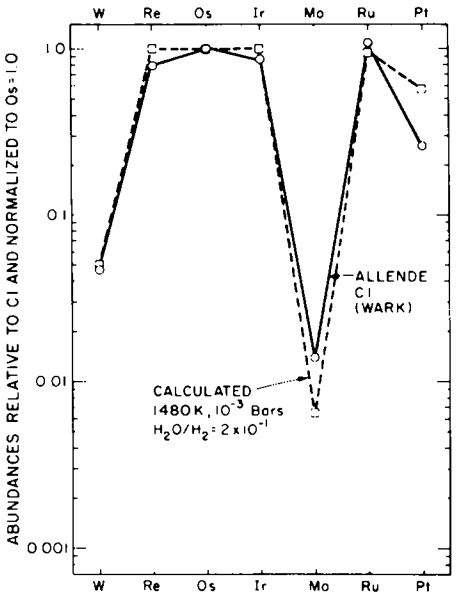

Fig. 6. Observed and calculated refractory metal abundances in the Allende FUN inclusion C1. The observed composition is from EDS/SEM analyses of metal grains by Wark [6].

slightly less-oxidizing conditions are required to reproduce Mo and W depletions of the same size.

The results in Figs. 3–6 (plus those not shown) illustrate several important points. First, there is good agreement between the calculated and observed metal abundance patterns for refractory inclusions from the four carbonaceous chondrites in which Mo and W depletions have been observed. Second, the temperatures calculated for the oxidation of the refractory metals are in the range 1450–1650 K. This temperature range is similar to the temperature range of 1438–1533 K for accretion of coarse-grained Type A inclusions (deduced from major element condensation calculations [1]). Furthermore the mean trace element enrichment factor for nine coarse-grained inclusions [1] also suggests an accretion temperature in the same range as the calculated oxidation temperatures. Third, the calculated (H_2O/H_2) ratios for oxidation of the refractory metals are in the same range: $\approx 10^{-2}$ to 10^{-1}. This coherence suggests that one single process may have been responsible for producing the higher (H_2O/H_2) ratios (if high-temperature oxidation is responsible for the metal abundance patterns in the refractory inclusions).

Last, the oxygen fugacities required to reproduce the observed Mo and W depletions vary in the same systematic fashion outlined in Fig. 1. Although the high-temperature oxidation of refractory metals is consistent with the observed Mo and W depletions in refractory inclusions; we should carefully examine alternative mechanisms to see if they can produce the Mo and W depletions and if they are as plausible as high-temperature oxidation.

4. Discussion

4.1. Possible alternative explanations of Mo and W depletions in refractory inclusions

One might think that uncertainties in elemental abundances and in thermodynamic data may cause Mo and W depletions in the calculated alloy compositions. Alternatively, it might be postulated that other chemical and physical processes in the solar nebula and on chondrite parent bodies may also produce similar Mo and W depletions in refractory inclusions. The first possibility is easily dismissed because uncertainties in elemental abundances [16] and thermodynamic data (as long as all stable species are considered) [21–28] are too small to produce significant changes in our calculated results. Although the second possibility cannot be unambiguously dismissed, a detailed analysis of alternative processes shows that none produces the same Mo and W depletion pattern found in the refractory inclusions.

For example, our calculations show that alloys formed at very low pressures ($P = 10^{-12}$ bars) may have small Mo depletions. At 10^{-3} bars and 1600 K, alloys with a Cl-normalized Ru/Os ratio of 0.8 have a Cl-normalized Mo/Os ratio of 0.95. At 10^{-12} bars and 1120 K, alloys with the same Cl-normalized Ru/Os ratio have a Mo/Os ratio of only 0.25. However, gas-solid equilibrium probably is not a valid assumption at such low pressures, which in any case are several orders of magnitude lower than the pressures calculated in recent models for the high-temperature regions of the solar nebula [34,35].

Fractional evaporation or condensation processes could also produce highly fractionated metal alloy compositions. For example, fractional condensation is postulated to produce the irregular Group II REE pattern in which both the most refractory (Er, Lu) and the most volatile REE (Eu, Yb) are depleted (see references in [1,2]). Because the formation of Group II REE patterns is postulated to involve dust-gas fractionation at high temperatures (e.g., ≈ 1676 K at 10^{-3} bars) at which refractory metal alloys also form, we have made several sets of fractional condensation calculations at pressures of 10^{-3} to 10^{-12} bars for metal alloys. A representative calculation shows the compositions of a metal alloy removed from equilibrium with the gas at 1675 K, and of the metals remaining in the gas (Fig. 7). The alloy removed from the gas is an "ultra"-refractory W-Re-Os alloy, while the alloy that eventually forms from the metals left in the gas is an Ir-Mo-Ru alloy. Neither of these alloys displays the same abundance patterns as Mo, W-depleted refractory inclusions (Figs. 3–6).

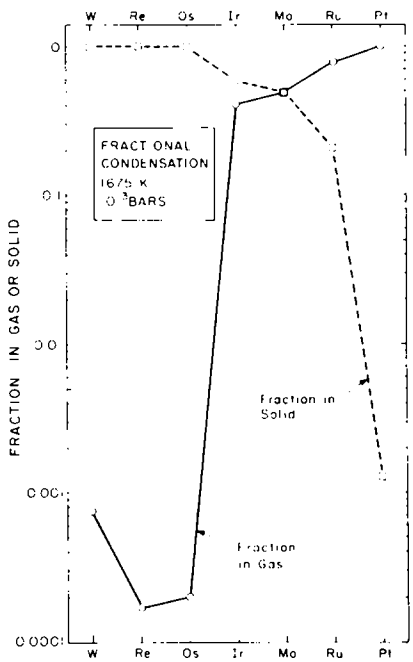

Fig. 7. The calculated composition of an "ultra"-refractory metal alloy produced by fractional condensation at 1675 K and 10^{-3} bars. The metals remaining in the gas condense to form an Ir-Mo-Ru alloy. Neither pattern matches the observed Mo and W depletions.

The chemical definition of oxidation is electron loss; therefore Mo and W could be oxidized by reacting with sulfur, which is a cosmically abundant element [16]. Furthermore, several observers have reported MoS_2 and WS_2 associated with complex, refractory metal-rich aggregates (Fremdlinge) in Allende inclusions [10,11,36,37]. Using thermodynamic data for MoS_2 from Robie et al. [38] and for WS_2, ReS_2, OsS_2, IrS_2, RuS_2, and PtS_2 from Mills [39], we have calculated equilibrium sulfur gas fugacities for the general reaction:

$$M(s) + S_2(g) = MS_2(s) \quad (8)$$

where M = W, Re, Os, Ir, Mo, Ru, Pt. These calculations show that the stabilities of these sulfides decrease in the order ($\log_{10} f_{S_2}$ values for 1000 K):

$$MoS_2(-12.8) > WS_2(-10.3) > RuS_2(-7.2) > ReS_2(-5.7) > OsS_2(-3.9) \approx IrS_2(-3.8) > PtS_2(-2.6) \quad (9)$$

Assuming ideal solution behavior in the metal alloy and sulfide, oxidation by $S_2(g)$ would always give Mo depletions that are several orders of magnitude larger than W depletions in the alloy. However, as noted by Fegley and Kornacki [2] in situ oxidation by sulfur merely redistributes Mo and W between metal and sulfide without depleting the assemblage in either element. This is graphically illustrated by the metal and sulfide particle studied by Palme and Wlotzka [11]. The bulk composition of this particle from neutron activation analysis and the metal composition from electron microprobe analysis are plotted in Fig. 8. The bulk particle has approximately chondritic relative abundances of refractory metals while the refractory metal is depleted in Mo. The Mo/Ru ratios for the bulk particle, metal, and sulfide phases are also given in Fig. 8. These ratios show that Mo is concentrated in the Ni-free sulfide, which Palme and Wlotzka [11] interpreted as a reaction product of metal and a S-bearing gas. This observation shows that physical removal of Mo- and W-bearing sulfides is necessary to produce Mo and W depletions in larger samples.

Alternatively, as a referee has suggested, Mo and W sulfurization (and depletion) could occur

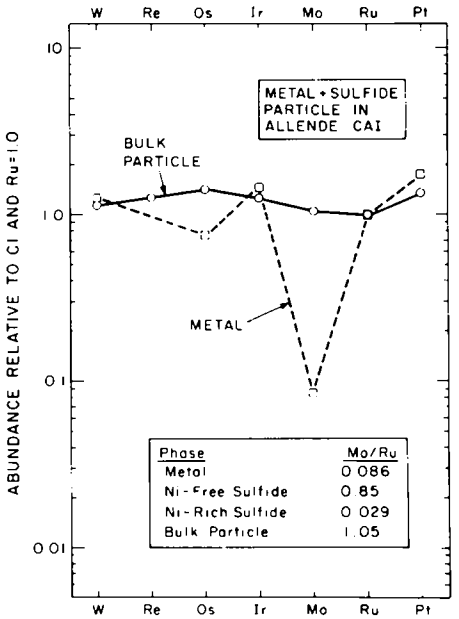

Fig. 8. The composition of a metal and sulfide particle described by Palme and Wlotzka [11]. The bulk composition (see Table 1) is from neutron activation. The metal and sulfide compositions are from electron microprobe analysis. There is no Mo or W depletion in the whole particle although Mo is concentrated in the sulfide and is depleted in the metal.

by condensation in a region of the solar nebula with a sulfur fugacity higher than the canonical value. However, our calculated results indicate that exactly the opposite would occur. Mo and W sulfide gases have not been reported [39] and apparently are very unstable; no thermodynamic data for them exist in standard compilations [22,23,25,26,38,39]. Thus, Mo and W loss by volatile sulfide gases appears very unlikely. However, condensation at enhanced sulfur fugacities does stabilize solid and liquid sulfides at high temperatures. CaS(s) is the first major Ca-bearing condensate ($\approx$ 1680 K, 10^{-3} bars) at sulfur fugacities $\approx 30\times$ greater than the canonical value ($H_2S/H_2 = 3 \times 10^{-5}$). Also, the FeS condensation temperature steadily increases as the sulfur fugacity increases; liquid FeS forms at $\approx$ 1480 K (10^{-3} bars) at a $10^3\times$ enhancement of the sulfur fugacity. This melt would have a very complex composition because it would dissolve sulfides of many elements (e.g., Mo, W, Mn, Ca, Ti, Si, etc.). MgS(s) forms at similar sulfur enrichments. Thus, Mo and

W enrichments (not depletions) would probably occur. Furthermore, the expected modal mineralogy is more similar to some phases in enstatite chondrites [40] than to CAIs [1]. Also note that because ≈ 100% of Ca, Mg, Fe, Ti, Si could be condensed as sulfides (depending on the sulfur fugacity), this condensate is not complementary to CAIs.

Carbonaceous chondrites also have been affected by thermal metamorphism [41] which could cause Mo and W loss as volatile gases or by reactions in the condensed phase. For example, Palme and Rammensee [42] noted that the Karoonda CV5 chondrite is depleted in Mo (Mo/Ir = 0.5 vs. the C1 value of 1.95). This is plausibly explained by oxidation by sulfur *and* physical removal of sulfide since Karoonda also has a low S content [42]. However, since Allende is not depleted in S relative to other C3 chondrites this mechanism cannot apply to it. There is also no evidence for secondary redistribution of Mo and W between CAIs and other constituents (e.g., chondrules and matrix) in Allende. Although the effect of planetary metamorphism on the chemistry of coarse-grained CAIs may be small [43], we have nonetheless considered this process for completeness. At temperatures ($T < 1000$ K) inferred for metamorphism of CV chondrites [43], thermodynamic calculations show that Mo and W loss by volatile gases produces larger W depletions (if oxyhalide gases are important) or equal W and Mo depletions (if oxide gases are important) in the metal phase. Condensed phase reactions forming Mo and W oxides or molybdate, tungstate solid solutions also are calculated to produce either approximately equal Mo and W depletions or greater W depletions in the metal, respectively. Neither pattern resembles those observed (Figs. 2–5).

Finally, aqueous alteration has also affected carbonaceous chondrites to varying degrees. However, petrographic and chemical studies indicate that CV3 chondrites such as Allende and Grosnaja have been relatively unaffected by aqueous alteration [41]. More stringent constraints are provided by oxygen isotopes in CV3 chondrites, which show no evidence for the extensive aqueous alteration which has affected CM and C1 chondrites [44].

4.2. Implications of Mo and W depletions for the oxidation state of refractory inclusions

Our proposal that the Mo and W depletions commonly observed in refractory inclusions are due to oxidation at high temperatures has implications for the oxidation state and abundances of other elements in CAIs. For example, the Ti^{3+}/Ti^{4+} ratio in fassaitic pyroxenes, the FeO content of spinels, the abundances of V, Ce, and U, the color of hibonite, and the presence of Fe^{3+}-bearing minerals such as andradite ($Ca_3Fe_2Si_3O_{12}$) all depend on the oxygen fugacity [45–48].

However, the oxidation state indicators which are present in Mo- and W-depleted refractory inclusions do not yield a consistent picture. The FUN inclusions TE and C1 have Mo and W depletions of similar magnitude but C1 has a Ce depletion (C1-normalized La/Ce ratio ≈ 3 [49]) while TE does not have a Ce depletion (C1-normalized La/Ce ratio ≈ 0.9 [9]). TE has a low V abundance (77 ppm), while Leo-1 has a higher V abundance (≈ 1200 ppm) [9]. These apparent discrepancies are representative of the difficulties involved in assigning a single oxygen fugacity to all components of a refractory CAI. Similar difficulties were noted by Wark and Wlotzka [50].

But is the concept of a *single* oxygen fugacity value for *all* components (e.g., siderophile elements and lithophile elements, rim and interior minerals, spinels and pyroxenes) really valid? Fegley and Kornacki [2] pointed out that different oxygen fugacity indicators may record fugacities prevailing at different times during the histories of the components of refractory inclusions. For example, the Fe^{3+}-bearing garnet andradite probably indicates the oxygen fugacity during the formation of rims on CAIs which apparently was much higher than the oxygen fugacity recorded by Fe^{2+}-bearing spinels and Ti^{3+}-bearing pyroxenes in the interiors of the same inclusions.

Fig. 9 illustrates several redox boundaries defined by Ti^{3+}/Ti^{4+} and Fe^{2+}/Fe^{3+} ratios (e.g., the boundary labelled Ti_2O_3-Ti_3O_5 is the minimum f_{O_2} at which Ti^{4+} exists; the boundary labelled Ti_3O_5-TiO_2 is the maximum f_{O_2} at which Ti^{3+} exists). The canonical solar nebula oxygen

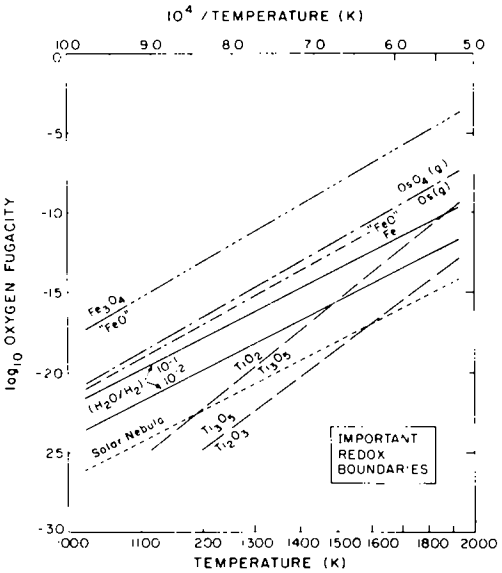

Fig. 9. Oxygen fugacity buffers for several Ti and Fe oxides compared to the canonical solar nebula oxygen fugacity. Oxygen fugacities corresponding to higher (H_2O/H_2) ratios are also shown. The line where 50% of all Os gases are present as $OsO_4(g)$ is also shown.

fugacity and the range of (H_2O/H_2) ratios corresponding to calculated Mo and W depletions in Figs. 3–6 are also illustrated. This figure shows that refractory minerals which are calculated to form at different temperatures in the solar nebula (e.g., perovskite at 1677 K (10^{-3} bars) [33] and Ti_3O_5 at 1409 K (10^{-3} bars) [1]) also form at different oxygen fugacities. Thus it is not unreasonable that refractory minerals found in CAIs (e.g., fassaitic pyroxene which may form instead of Ti_3O_5 [1], V- and Fe-bearing spinels, perovskite, hibonite) will record different oxygen fugacities simply because they formed at different temperatures.

Similar considerations apply to the REE which were originally proposed as oxygen fugacity indicators by Boynton [45]. He first showed that Ce is more volatile in oxidizing gases than are the other REE (relative to La) and suggested that Ce depletions (e.g., relative to the Cl-normalized La/Ce ratio) are an indicator of high oxygen fugacities. However, the only inclusion we know of with both Mo and W depletions as well as a Ce depletion is the FUN inclusion C1 [8,49]. Furthermore our preliminary REE chemical equilibrium calculations (which will be described elsewhere) indicate that other inclusions with large Mo and W depletions should also have Ce depletions if the REE *last* equilibrated with the gas phase at the same T, P, and f_{O_2} as that calculated to match the Mo and W depletions in the inclusions. The apparently discordant results may simply indicate REE equilibration under less oxidizing conditions at a different time and/or place. Because refractory metals and REE probably were carried into coarse-grained Allende inclusions in different components [1], and probably reacted with nebular gas at different rates this explanation is not unreasonable. We conclude that the concept of a single oxygen fugacity, which is characteristic of an entire CAI, is probably not valid. The separate question of which (and how many) potential oxygen fugacity indicators may record a general trend toward more or less oxidizing conditions is beyond the scope of this paper.

4.3. Oxidizing conditions in the solar nebula

A frequently suggested mechanism for producing oxidizing conditions in the solar nebula is enhancement of the dust to gas ratio [51]. Simple mass balance considerations illustrate why this suggestion is revived almost perenially. Approximately 20% of all oxygen resides in anhydrous dust ($MgO + SiO_2 + FeO + CaO + Al_2O_3$), $\approx 20\%$ is in $H_2O(g)$, and the remaining 60% is in CO(g). This latter oxygen is essentially locked up in CO(g) because at high temperatures CO(g) is thermodynamically stable and at low temperatures the CO to CH_4 conversion is kinetically inhibited in the solar nebula [52].

Table 5 shows the effect of dust and ice enrichments on oxygen fugacity in the solar nebula. The mole fractions and weight percentages of dust and ice corresponding to their respective enrichments are also given. Because oxygen fugacity is expressed as the corresponding (H_2O/H_2) ratio, the effect of these enrichments on f_{O_2} at different temperatures can be deduced from Fig. 9. Table 5 illustrates that dust or ice enrichments on the order of $\leqslant 50\times$ are sufficient to produce fairly large Mo depletions in refractory metal alloys (see

TABLE 5

Effects of dust [a] and ice [b] enrichments on (H_2O/H_2) in the solar nebula

Dust enrichment	X_{dust}	Dust (wt.%)	(H_2O/H_2)	Ice enrichment	X_{ice}	Ice (wt.%)	(H_2O/H_2)
1 (solar)	2×10^{-4}	0.5	5×10^{-4}	1 (solar)	2.6×10^{-4}	0.2	5×10^{-4}
50	9.6×10^{-3}	20	1.6×10^{-2}	50	1.3×10^{-2}	9.4	1.5×10^{-2}
250	0.05	55	7.6×10^{-2}	250	0.06	34	7.6×10^{-2}
500	0.09	71	0.15	500	0.12	51	0.15
750	0.13	78	0.23	750	0.16	61	0.23
1000	0.16	83	0.30	1000	0.21	67	0.30

[a] Dust = $MgO + SiO_2 + FeO + CaO + Al_2O_3$.
[b] Ice excludes oxygen in dust and CO(g) [52].
X = mole fraction.

Fig. 1). Larger enrichments of $\approx 500\times$ are required to produce large Mo and W depletions. Table 5 also shows that the enrichment factors for ice and dust mixtures are only slightly smaller than enrichment factors for the separate components unless ice and dust are present in grossly non-solar proportions.

The enrichment of dust and ice has several consequences in addition to increasing the oxygen fugacity, including increases in the opacity, viscosity, and coagulation rate in this region of the nebula. The increased oxygen fugacity (from partial or total vaporization of the dust and ice) would affect not only the oxidation of Mo and W but also the trace element and bulk chemistry [53] of the distillation residues and recondensates. Also note that each evaporating dust grain will create its own locally-oxidizing environment independent of the dust/gas ratio in the solar nebula [5].

A second mechanism for producing locally-oxidizing environments in evaporating dust grains is by chemical oxidizing agents. If refractory metal nuggets are formed during the evaporation and partial melting of primitive dust aggregates [2,34], this process could have been aided by the chemical fluxing of the refractory metals. Extractive metallurgical practice utilizes oxidizing agents as fluxes [2]; these agents also could cause Mo and W depletions. Fegley and Kornacki [2,33,34] have suggested that evaporation, fluxing, and partial melting are important for the formation of refractory metal nuggets in CAIs, a model supported by the demonstration of Brownlee et al. [54] that similar processes are apparently responsible for refractory metal nuggets in FeO-bearing cosmic spherules found in deep-sea sediments.

Our conclusion that the observed Mo and W depletions are caused by high-temperature oxidation in the solar nebula is compatible with both mechanisms discussed above. At present the available data are insufficient to select between them.

5. Summary

We have shown that Mo and W depletions are common in a suite of 16 CAIs from carbonaceous chondrites. Twelve inclusions from the Allende (CV3), Grosnaja (CV3), Leoville (CV3), and Ornans (CO3) chondrites have Mo depletions ranging from $\approx 25\%$ to $40\times$ the C1-normalized refractory metal ratios. Six of these 12 inclusions also have W depletions of $\approx 25\%$ to $25\times$ the C1 metal ratio. The Mo depletion is always larger than the W depletion in the same inclusion. The occurrence of Mo and W depletions in several different carbonaceous chondrites, in inclusions of different mineralogical types and with different REE patterns, in FUN inclusions and "normal" inclusions, and in different components (e.g., refractory metal grains and Fremdlinge) of CAIs strongly suggests that the process responsible for the Mo and W depletions was widespread in the solar nebula.

Our calculations of refractory metal alloy compositions over a wide range of T, P, and f_{O_2} condi-

tions show that alloys with the same characteristic Mo and W depletion pattern (as seen in the inclusions) are produced only at oxygen fugacities 10^3–$10^4\times$ greater than the canonical solar nebula oxygen fugacity. Several other potential alternative processes such as fractional condensation, oxidation by sulfur, and metamorphism were studied, but are inadequate for explaining the observed depletion patterns.

Assuming that high-temperature oxidation is responsible for the Mo and W depletions, we argue that oxidized metal can coexist (although not at equilibrium) with less oxidized components of the same inclusion. That is, the concept of a single oxygen fugacity which is characteristic of all components of a CAI is not valid. Furthermore, we note that the inferred oxidation can occur during the evaporation and partial melting of a proto-CAI. A similar mechanism has been independently proposed for the origin of refractory metal nuggets in deep-sea FeO-bearing cosmic spherules [54]. However, the observed Mo and W depletions and our calculations also are consistent with condensation in an oxidizing environment.

Acknowledgements

We thank H. Kruse for assisting with progamming the code METKON. We also thank H. Wänke for constructive comments; W.V. Boynton, J.W. Larimer, and D.A. Wark for constructive reviews; B.F. also thanks A.S. Kornacki for stimulating his interest in the oxidation state of Allende inclusions and L. Manzi for preparation of this manuscript.

References

1 L. Grossman, Refractory inclusions in the Allende meteorite, Annu. Rev. Earth Planet. Sci. 8, 559–608, 1980.
2 B. Fegley, Jr. and A.S. Kornacki, The geochemical behavior of refractory noble metals and lithophile trace elements in refractory inclusions in carbonaceous chondrites, Earth Planet. Sci. Lett. 68, 181–197, 1984.
3 M. Blander, L.H. Fuchs, C. Horowitz and R. Land, Primordial refractory metal particles in the Allende meteorite, Geochim. Cosmochim. Acta 44, 217–223, 1980.
4 B. Mason and S.R. Taylor, Inclusions in the Allende meteorite, Smithsonian Contrib. Earth Sci. 25, 1982.
5 H. Palme, F. Wlotzka, K. Nagel and A. El Goresy, An ultra-refractory inclusion from the Ornans carbonaceous chondrite, Earth Planet. Sci. Lett. 61, 1–12, 1982.
6 D.A. Wark, The Allende meteorite: information from Ca-Al-rich inclusions on the formation and early evolution of the solar system, 385 pp., Ph.D. Thesis, University of Melbourne, Parkville, Vic., 1984.
7 H. Palme, B. Spettel and F. Wlotzka, Fractionation of refractory metals in Ca,Al-rich inclusions from carbonaceous chondrites, Meteoritics 17, 267, 1982.
8 D.A. Wark and G.J. Wasserburg, Anomalous mineral chemistry of Allende FUN inclusions C1, EK-141 and Egg3, Lunar Planet. Sci. XI, 1214–1216, 1980.
9 H. Palme, F. Wlotzka, B. Spettel and H. Wänke, in preparation.
10 L.H. Fuchs and M. Blander, Refractory metal particles in refractory inclusions in the Allende meteorite, Proc. 11th Lunar Planet. Sci. Conf., pp. 929–944, 1980.
11 H. Palme and F. Wlotzka, A metal particle from a Ca,Al-rich inclusion from the meteorite Allende, and the condensation of refractory siderophile elements, Earth Planet. Sci. Lett. 33, 45–60, 1976.
12 H. Wänke, H. Baddenhausen, H. Palme and B. Spettel, On the chemistry of the Allende inclusions and their origin as high temperature condensates, Earth Planet. Sci. Lett. 23, 1–7, 1974.
13 B. Dominik, E.K. Jessberger, Th. Staudacher, K. Nagel and A. El Goresy, A new type of white inclusion in Allende: petrography, mineral chemistry, ^{40}Ar-^{39}Ar ages, and genetic implications, Proc. 9th Lunar Planet. Sci. Conf., pp. 1249–1266, 1978.
14 R.N. Clayton, G.J. MacPherson, I.D. Hutcheon, A.M. Davis, L. Grossman, T.K. Mayeda, C. Molini-Velsko and J.M. Allen, Two forsterite-bearing FUN inclusions in the Allende meteorite, Geochim. Cosmochim. Acta 48, 535–548, 1984.
15 H. Palme and F. Wlotzka, A Ca,Al-rich inclusion from the Leoville (CV3) meteorite, Meteoritics 14, 508–511, 1979.
16 E. Anders and M. Ebihara, Solar-system abundances of the elements, Geochim. Cosmochim. Acta 46, 2363–2380, 1982.
17 A. El Goresy, H. Palme, H. Yabuki, K. Nagel and P. Ramdohr, A refractory inclusion from the Essebi (CM2) carbonaceous chondrite, Lunar Planet. Sci. XIV, 173–174, 1983.
18 R.H. Becker and S. Epstein, Silicon and oxygen isotopes in some selected Allende inclusions, Lunar Planet. Sci. XII, 56–58, 1981.
19 B. Mason and P.M. Martin, Minor and trace element distribution in melilite and pyroxene from the Allende meteorite, Earth Planet. Sci. Lett. 22, 141–144, 1974.
20 F. Van Zeggeren and S.H. Storey, The Computation of Chemical Equilibria, Cambridge University Press, New York, N.Y., 1970.
21 R. Hultgren, P.D. Desai, D.T. Hawkins, M. Gleiser, K.K. Kelley and D.D. Wagman, Selected Values of the Thermo-

dynamic Properties of the Elements, American Society for Metals, Ohio, 1973.
22 JANAF Thermochemical Tables, 2nd ed., No NSRDS-NBS-37, D.R. Stull and H. Prophet, eds., U.S. Government Printing Office, Washington, D.C., 1971.
23 V.P. Glushko and V.A. Medvedev, ed., Termicheskie Konstanty Veshchestv, Akademiya Nauk SSSR, Moscow, 1965–1983.
24 M.S. Chandrasekharaiah, M.D. Karkhanavala and S.N. Tripathi, The pressure of iridium oxides over iridium at high temperatures in 1 atm. of dry oxygen, J. Less Common Metals 80, P9–P17, 1981.
25 K.K. Kelley, Contributions to the data on theoretical metallurgy, XIII. High-temperature heat-capacity and entropy data for the elements and inorganic compounds, U.S. Bur. Mines Bull. 584, 1960.
26 D.D. Wagman, W.H. Evans, V.B. Parker, I. Halow, S. Bailey and R.H. Schumm, Selected values of chemical thermodynamic properties, U.S. Natl. Bur. Standards Tech. Note 270-4, 1969.
27 J.C.B. Alcock and G.W. Hooper, Thermodynamics of the gaseous oxides of the Pt-group metals, Proc. R. Soc. London 254, 551–561, 1960.
28 M.H. Ortner, Infrared spectrum and thermodynamic properties of ruthenium tetroxide, J. Chem. Phys. 34, 556–558, 1961.
29 D.G. Fraser and W. Rammensee, Activity measurements by Knudsen cell mass spectrometry – the system Fe-Co-Ni and implications for condensation processes in the solar nebula, Geochim. Cosmochim. Acta 46, 549–556, 1982.
30 W. Rammensee, H. Palme and B. Fegley, Determination of activities of Ni, Co, Cr, V in refractory metal alloys, in preparation.
31 J.K.M. Gibson, Thermochemistry of acid-base stabilized transition metal alloys by carbide and nitride equilibria and Knudsen effusion vapor pressures, 146 pp., Ph.D. Thesis, University of California, Berkeley, Calif., 1983.
32 L. Brewer, Molybdenum: physico-chemical properties of its compounds and alloys, IAEA At. Energy Rev. 7, 1980.
33 A.S. Kornacki and B. Fegley, Jr., Origin of spinel-rich chondrules and inclusions in carbonaceous and ordinary chondrites, Proc. 14th Lunar Planet. Sci. Conf., J. Geophys. Res. 89, B588–B596, 1984.
34 A.G.W. Cameron and M.B. Fegley, Nucleation and condensation in the primitive solar nebula, Icarus 52, 1–13, 1982.
35 G.E. Morfill, Some cosmochemical consequences of a turbulent protoplanetary cloud, Icarus 53, 41–54, 1983.
36 A. El Goresy, K. Nagel and P. Ramdohr, Fremdlinge and their noble relatives, Proc. 9th Lunar Planet. Sci. Conf., pp. 1279–1303, 1978.
37 L.H. Fuchs and M. Blander, Molybdenite in calcium-aluminum-rich inclusions in the Allende meteorite, Geochim. Cosmochim. Acta 41, 1170–1175, 1977.
38 R.A. Robie, B.S. Hemingway and J.R. Fisher, Thermodynamic properties of minerals and related substances at 298.15 K and 1 bar (10^5 pascals) pressure and at higher temperatures, U.S. Geol. Surv. Bull. 1452, 1979.
39 K.C. Mills, Thermodynamic Data for Inorganic Sulfides, Selenides and Tellurides, Butterworths, London, 1974.
40 K. Keil, Mineralogical and chemical relationships among enstatite chondrites, J. Geophys. Res. 73, 6945–6976, 1968.
41 H.Y. McSween, Jr., Are carbonaceous chondrites primitive or processed?, Rev. Geophys. Space Phys. 17, 1059–1078, 1979.
42 H. Palme and W. Rammensee, The cosmic abundance of molybdenum, Earth Planet. Sci. Lett. 55, 356–362, 1981.
43 H.Y. McSween, Jr., Petrographic variations among carbonaceous chondrites of the Vigarano type, Geochim. Cosmochim. Acta 41, 1777–1790, 1977.
44 R.N. Clayton and T.K. Mayeda, The oxygen isotope record in Murchison and other carbonaceous chondrites, Earth Planet. Sci. Lett. 67, 151–161, 1984.
45 W.V. Boynton, Rare-earth elements as indicators of supernova condensation, Lunar Planet. Sci. IX, 120–122, 1978.
46 W.V. Boynton and C.C. Cunningham, Condensation of refractory lithophile trace elements in the solar nebula and in supernovae, Lunar Planet. Sci. XII, 106–108, 1981.
47 E. Dowty and J.R. Clark, Crystal structure refinement and optical properties of a Ti^{3+} fassaite, Am. Mineral. 58, 230–242; 962–964, 1973.
48 E. Stolper and P. Ihinger, The color of meteoritic hibonite: an indicator of oxygen fugacity, Lunar Planet. Sci. XIV, 749–750, 1983.
49 R. Conard, A study of the chemical composition of Ca,Al-rich inclusions from the Allende meteorite, 129 pp., M.S. Thesis, Oregon State University, 1976.
50 D.A. Wark and F. Wlotzka, The paradoxical metal compositions in Leo-1, a Type B1 Ca-Al-rich inclusion from Leoville, Lunar Planet. Sci. XIII, 833–834, 1982.
51 H.Y. McSween, Jr., Chemical and petrographic constraints on the origin of chondrules and inclusions in carbonaceous chondrites, Geochim. Cosmochim. Acta 41, 1843–1850, 1977.
52 J.S. Lewis and R.G. Prinn, Kinetic inhibition of CO and N_2 reduction in the solar nebular, Astrophys. J. 238, 357–364, 1980.
53 H.A. Bartholomay and J.W. Larimer, Dust-gas fractionation in the early solar system, Meteoritics 17, 180–181, 1982.
54 D.E. Brownlee, B.A. Bates and M.M. Wheelock, Extraterrestrial platinum group nuggets in deep-sea sediments, Nature 309, 693–694, 1984.